FOCUSED ISSUE FEATURE

George V. Eleftheriades and Michael Selvanayagam

Transforming Electromagnetics Using Metamaterials

Electromagnetic metamaterials are artificially structured media with unusual electromagnetic properties that can be engineered from the radio-frequency (RF) and microwave range all the way up to optical frequencies. In its present form, the field of metamaterials is just over ten years old but has already attracted intense interest from many research groups around the globe. Suddenly, classical electromagnetism took on a fresh and exciting perspective, revealing that there are fascinating phenomena still waiting to be discovered and corresponding applications to be invented. In particular, all this excitement is associated with the notion of the macroscopic constitutive parameters, such as the permittivity and permeability. What would be possible if we were able to synthesize electromagnetic materials with

George V. Eleftheriades (gelefth@waves.utoronto.ca), IEEE Fellow, and Michael Selvanayagam are with the Department of Electrical and Computer Engineering, University of Toronto, 10 King's College Road, Toronto, ON M5S 3G4, Canada.

Digital Object Identifier 10.1109/MMM.2011.2181446
Date of publication: 9 March 2012

 1527-3342/12/$31.00©2012 IEEE

arbitrarily valued constitutive parameters? The richness of this possibility becomes more evident when we recall that material parameters can be anisotropic (varying with direction) or spatially inhomogeneous (varying from point to point). Moreover, they can attain values previously not considered (i.e., negative or close to zero), and they can even mix together the electric and magnetic response of a material (chirality).

Artificial Dielectrics and Metamaterials

Typically, metamaterials are periodic structures consisting of metallodielectric scatterers having a periodicity that is much smaller than the impinging and dominant Bloch wavelengths. Here it should be noted that a wave in a periodic structure [one-dimensional (1-D) for clarity] can be described by

$$f(x+d) = f(x)e^{-j\beta_{\text{Bloch}}x}, \tag{1}$$

where d is the periodicity and β_{Bloch} is defined as the Bloch propagation constant [1]. These constituent scatterers behave like artificial molecules that scatter an incident electromagnetic wave. The corresponding interaction can be represented with macroscopic effective material parameters such as the permittivity, the permeability, and the refractive index. Although the term "metamaterial" now used to describe such structures is relatively new, the basic concept has been around since at least the late 1940s under the name "artificial dielectric." Specifically at that time, Winston E. Kock of Bell Laboratories introduced the concept of the artificial dielectric in order to realize lightweight lenses at microwave frequencies (in the 3–5 GHz range), where the wavelength is long (several centimeters) and the corresponding natural dielectric lenses are bulky and heavy [2]. The corresponding artificial molecules were electrically small metallic disks periodically arranged in a concave lens shape. When a plane wave impinges on such an artificial lens with the electric field polarized along the disks, charges separate on the disks thus creating small dipoles, similar to the molecular dipoles induced in nonpolar dielectrics by an impressed field. Kock used simple Lorentz theory to describe his artificial dielectrics summarized by $\varepsilon_{\text{eff}} = \varepsilon_o + N\alpha$, where ε_o is the permittivity of free space, ε_{eff} is the effective permittivity, N is the number of disks per volume, and α is the polarizability of the disks. Using this approach, broadband effective permittivities could be obtained due to the nonresonant nature of the (small) disks (the polarizability is fairly constant with frequency). A comprehensive review of artificial dielectrics, including a rigorous mathematical treatment, from that era can be found in [3]. Moreover, it is worth mentioning some early relevant work on effective media, such as that by Bose, who in 1898 used man-made twisted fibers (jute) to rotate the polarization of electromagnetic waves, thus emulating naturally occurring chiral media such as sugar [4]. In a related effort, Lindman in 1914 studied artificial chiral media formed by an ensemble of small wire helices [5]. It could also be mentioned that in the 1950s, Von Hippel utilized a lumped resistor-inductor-capacitor (RLC resonant-circuit model for characterizing the Lorentzian response of dielectric media [6].

In this context, metamaterials can be defined as a superset of artificial dielectrics with electromagnetic properties, including those that are inaccessible in nature or are difficult to obtain. Perhaps the most representative metamaterial is the so-called left-handed (LH) one (also known as a "negative-refractive-index (NRI)" or a "double negative" medium), which is characterized by a simultaneously negative permittivity and permeability, thus implying a negative index of refraction. These media were theoretically studied by Victor Veselago in the 1960s [7]. To access these unusual material parameters, the constituent unit cells need to be resonant, which leads to dispersion. Consequently, unlike Kock's artificial dielectrics, today's metamaterials are usually dispersive in nature.

The Split-Ring-Resonator/Wire Left-Handed Metamaterial

In his visionary paper, Veselago demonstrated that a hypothetical medium with a negative permittivity and permeability is compatible with Maxwell's equations and described the electromagnetic properties of such media. For example, he pointed out that in such media, the electric field $\overline{E}$, the magnetic field $\overline{H}$, and the propagation vector $\overline{k}$ would follow an LH rule (hence the designation "LH media") and that the phase and group velocities would be

In its present form, the field of metamaterials is just over ten years old but has already attracted intense interest from many research groups around the globe.

antiparallel, implying a negative index of refraction. However, Veselago did not conclusively prescribe any specific structure that would exhibit these properties. He recognized that plasmas could be used to obtain a negative permittivity, and he speculated that some kind of a magnetic plasma (not available naturally) would be needed to obtain a negative permeability. The solution to the problem of realizing such an LH or NRI medium was solved three decades later by Shelby, Smith, and Schultz [8], inspired by the work of John Pendry. The structure that was used consisted of an array of strip wires to synthesize a negative permittivity and a structure called the "split-ring resonator," a capacitively loaded loop, to synthesize a negative permeability, as shown in Figure 1. The use of an array of inductive wires to synthesize artificial dielectrics with plasma-like behavior was previously reported by Walter Rotman [9] (although Rotman never explored the $\varepsilon < 0$ region) and independently by John Pendry, who boldly put forward the idea that the wires can exhibit a negative permittivity [10]. The use of split-ring resonators to synthesize negative permeability media was also suggested by John Pendry in a seminal paper published in *IEEE Transactions on Microwave Theory and Techniques* [11]. Nevertheless, it should be noted that artificial media made of capacitively loaded loops were also suggested by Sergei Schelkunoff in 1952 [12]. However, Schelkunoff suggested these particles as a means of synthesizing a large positive permeability (and not a negative one), but he recognized that such magnetic artificial materials would be quite dispersive.

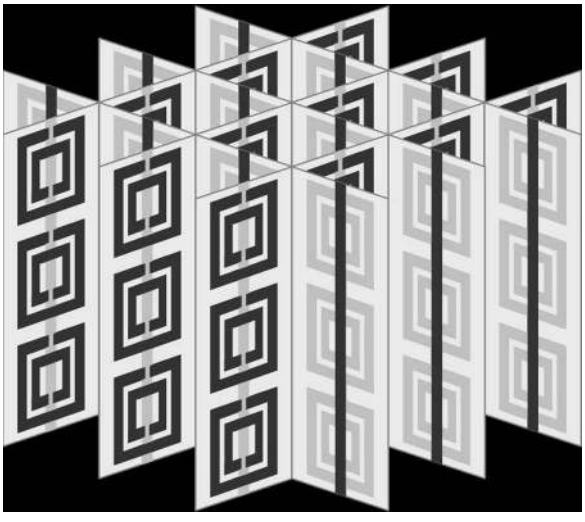

Figure 1. *The split-ring resonator and wire medium. The electric field is polarized along the wires ($\varepsilon < 0$) while the magnetic field permeates the split-ring resonators ($\mu < 0$) [18].*

The Negative-Refractive-Index Transmission-Line Metamaterial

An alternative method for realizing LH metamaterials consists of loading a host transmission-line (TL) medium with reactive elements [13]–[15]. For example, for synthesizing an LH metamaterial in two dimensions, a host microstrip line network can be loaded periodically with series capacitors and shunt inductors, as shown in Figure 2. Such loaded lines support backward waves. More precisely, the fundamental spatial harmonic is a backward one and becomes dominant near the Gamma point, i.e., for small phase-shifts per unit cell [16].

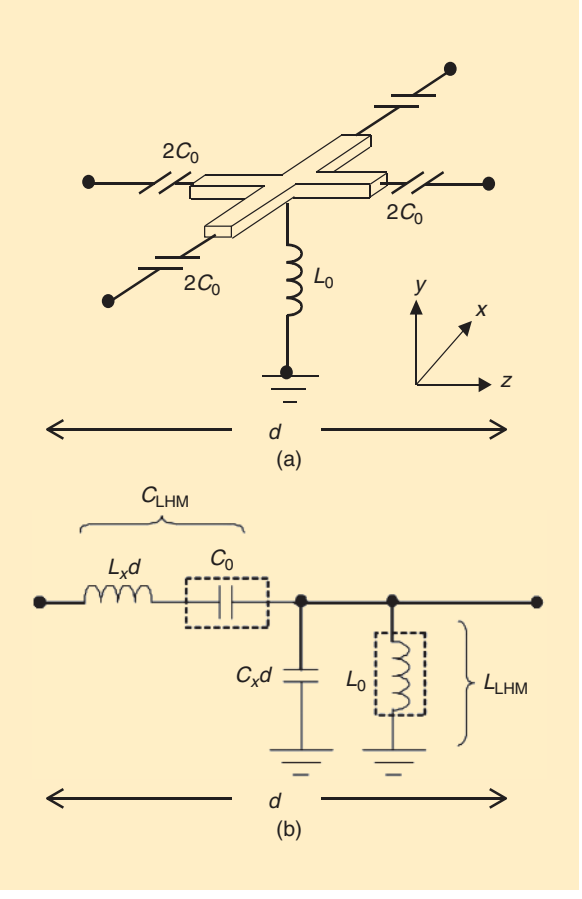

Figure 2. *(a) Unit cell for the 2-D NRI-TL metamaterial. A host TL is loaded periodically with series capacitors and shunt inductors. (b) In the limit $\beta d \to 0$, the interconnecting TLs can be replaced by an equivalent series inductance $L_x d$ and shunt capacitance $C_x d$. This yields a band-pass filter type of a unit cell, which contains both an LH and an RH response. A modified version of this 1-D equivalent circuit can be used to represent axial propagation in the 2-D NRI-TL medium (see [13] for details).*

A typical dispersion diagram for a 1-D NRI-TL medium is shown in Figure 3. See [17] and [18] for the complete two-dimensional (2-D) dispersion characterization.

As shown in Figure 3, the lower band is LH (backward wave), in which the phase velocity is negative (the wavefronts move toward the source), but the group velocity (slope) is positive (the power moves away from the source). In this lower band, the loading elements C_o and L_o dominate, whereas at higher frequencies, the underlying TL dominates, yielding a right-handed (RH) (forward-wave) band. Typically, these two bands are separated by a stopband, which is delimited by two plasma frequencies f_c^{μ} and f_c^{ε}. These are the frequencies that correspond to the series and shunt resonance in Figure 2(b) (i.e., the effective permeability $\mu_{\text{eff}}(\omega)$ and permittivity $\varepsilon_{\text{eff}}(\omega)$ vanish). These cutoff frequencies are readily determined to be

$$f_c^{\mu} = \frac{1}{2\pi\sqrt{L_x C_o}\,d}, \tag{2}$$

$$f_c^{\varepsilon} = \frac{1}{2\pi\sqrt{L_o C_x}\,d}, \tag{3}$$

where the characteristic impedance of the host TL is $Z_x = \sqrt{L_x/C_x}$. By equating f_c^{μ} and f_c^{ε}, the stopband in Figure 3(a) can be closed, thus allowing access of phase shifts around the zero mark, as shown in Figure 3(b) (i.e., a zero index of refraction but with the medium still remaining matched). The condition for a closed stopband is therefore determined to be

$$Z_x = \sqrt{\frac{L_o}{C_o}}. \tag{4}$$

This closed stopband condition (4) was derived in [13, (29)] and [14]. Under this condition, the effective propagation constant can be approximated by

$$\beta_{\text{Bloch}} \approx \omega\sqrt{L_x C_x} - \frac{1}{\omega\sqrt{(L_o d)(C_o d)}}. \tag{5}$$

This expression can be interpreted as the sum of the phase incurred by the host TL (forward wave) and a uniform backward wave line. Likewise, the corresponding effective index of refraction would be $n = c\beta_{\text{Bloch}}/\omega$. Because there is both a backward (LH) and a forward (RH) frequency response in the dominant Bloch propagation constant as given by (5), in the microwave literature, the TL media of Figure 2 are also known by the name "composite-right-left-handed (CRLH)" [14] media.

As mentioned previously, NRI-TL-based metamaterials enjoy wide LH (backward-wave) passbands and low insertion losses. The origin of these advantages stems from the fact that their constituent capacitor-inductor (*C-L*) resonators are tightly coupled together through their electrical connections [19].

Negative Refraction

One of the most striking phenomena associated with metamaterials is negative refraction, which is supported by LH isotropic metamaterials that are characterized by a negative index of refraction. One way to

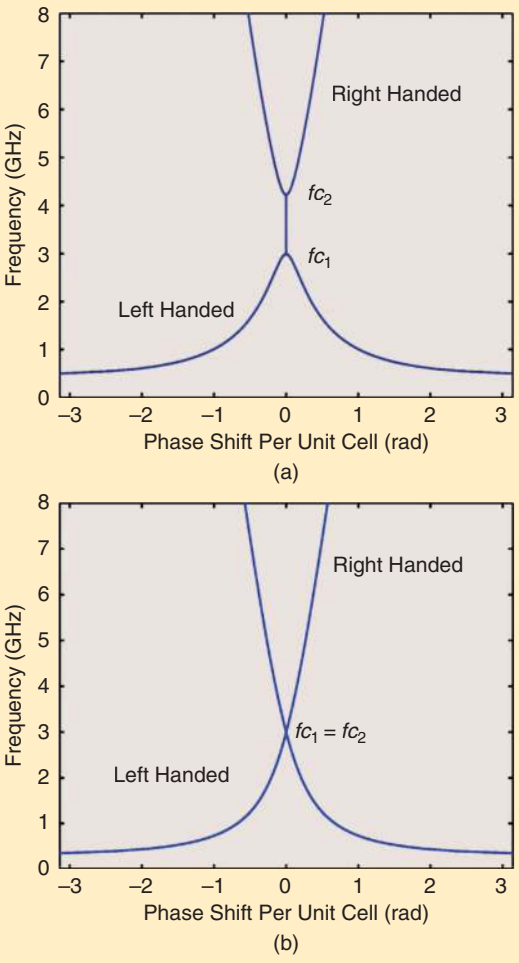

Figure 3. *Sample dispersion diagrams for a 1-D NRI-TL. (a) Open stopband case. The interconnecting line is characterized by a phase shift of $\theta = 0.25$ rad at 3 GHz and $Z_x = 50\ \Omega$, whereas the series loading capacitors are $C_o = 4.24$ pF and the shunt loading inductors are $L_o = 5.3$ nH. The lower band is LH (backward wave, negative index), whereas the upper one is right handed (forward wave, positive index). The stopband between these two bands is delimited by the two plasma frequencies f_{c1}, f_{c2}. The size of this stopband is determined by the degree of mismatch between the constituent forward and backward lines: $f_{c2}/f_{c1} = Z_x/\sqrt{L_o/C_o}$. (b) Closed stopband case. The interconnecting line is characterized by a phase shift of $\theta = 0.25$ rad at 3 GHz and $Z_x = 50\ \Omega$ whereas the series loading capacitors are $C_o = 4.24$ pF and the shunt loading inductors are $L_o = 10.6$ nH such that the closed stopband condition $Z_o = \sqrt{L_o/C_o}$ is satisfied. Note that this case gives access to a zero index of refraction at $f_{c1} = f_{c2} \cong 1/(C_o Z_x \theta)$ where the artificial medium is matched (nonzero group velocity).*

One of the most exciting propositions in metamaterial research has been that of imaging beyond the diffraction limit.

understand negative refraction is through the notion of phase matching, as explained in Figure 4. Since Snell's law is a manifestation of phase matching of the transverse propagation vector at the interface between two dielectrics, Figure 4 readily suggests that the LH medium should be characterized by a negative refractive index.

Based on negative refraction, a new class of lenses can be envisioned. Perhaps the most celebrated one is the Veselago-Pendry lens, which is shown in Figure 5. As shown, this lens can achieve point-to-point focusing through negative refraction, despite the fact that its two surfaces are flat. Moreover, the lens can overcome the diffraction limit, as explained in the next section.

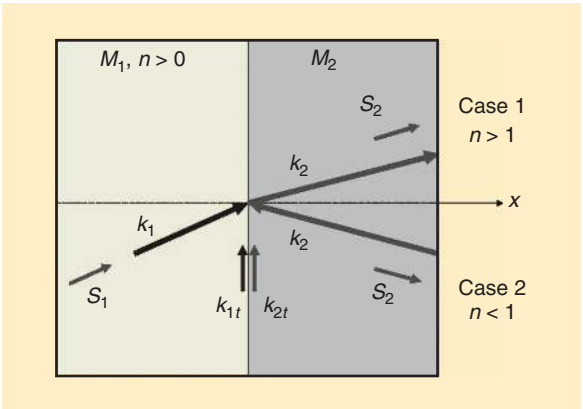

Figure 4. *Negative refraction of a plane wave incident from a regular dielectric to another regular dielectric (Case 1) or an NRI medium (Case 2). The arrows on the rays represent the propagation vectors; observe the underlying phase matching of the tangential components of these vectors in Case 2. Another implied principle is that the Poynting Vector* **S** *should point away from the interface in the second medium (from [13]).*

The Veselago-Pendry Superlens

One of the most exciting propositions in metamaterial research has been that of imaging beyond the diffraction limit. This excitement was stirred when John Pendry, in his ground-breaking work [20], proposed that the Veselago lens of Figure 5 could be considered to act as a perfect lens. This proposition should be understood in the context of operating the Veselago lens as a microscope. In this setting, what limits the resolution is the lost transverse wave vectors k_x (assuming 2-D propagation for simplicity). The propagating waves $k_x < k_o$, corresponding to large propagation angles with the optical axis, will not be collected by the lens aperture and will be lost. However, if the diameter of the lens is large enough, all these propagating waves will be collected and focused at the image plane according to the ray diagram of Figure 5. However, even in this case, the resolution of a conventional lens would be limited because the evanescent waves $k_x > k_o$ (near field) will not make it to the image plane because of their strong exponential attenuation with distance. Therefore, at best, the resolution of a conventional lens/microscope will be limited by $2\pi/k_o = \lambda_o$, i.e., by the wavelength of the electromagnetic wave used for imaging.

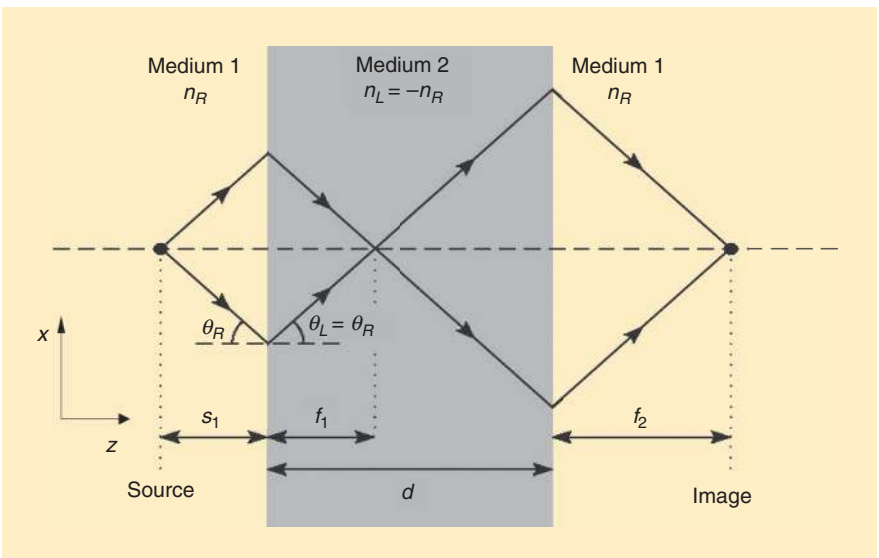

Figure 5. *A Veselago-Pendry lens made out of a slab of an NRI medium. As shown, negative refraction is utilized in order to focus a point to a point. This leads to a lens with flat surfaces and no optical axis. The rays (defined with respect to the Poynting vector, i.e., power flow, in this figure) converge to the same point when the relative index is n=−1, thus leading to aberration-free focusing. The thickness of the lens d is half the distance from the source to the image [57].*

For the Veselago-Pendry lens, the propagating waves, $k_x < k_o$ are perfectly restored at the image plane according to the ray diagram of Figure 5. In this case, there is perfect matching (no reflections) for all k_x components, which is beneficial given that refraction at oblique incidence on a conventional (positive index) dielectric leads to reflections (even if the dielectric were matched at normal incidence). What is even more surprising though is the fact that the evanescent-wave components, $k_x > k_o$ are also matched and the corresponding transmission

coefficient from the source to the image plane is one (e.g., see [18, pp. 85–87]). Therefore, at least under ideal conditions, the Veselago lens restores a perfect image.

The first experimental demonstration of such imaging beyond the diffraction limit with a Veselago-Pendry lens has been reported in [21] using a 2-D in-plane lens made out of a 2-D NRI-TL metamaterial. Moreover, the first volumetric Veselago-Pendry superlens using TL metamaterials was reported in [22] using a layer-by-layer NRI-TL. The resulting structure is isotropic for waves having their magnetic fields polarized perpendicularly to the layers. The corresponding structure is shown in Figure 6 and consists of layers of NRI coplanar-strip TLs. In order to reduce the losses, high-Q chip capacitors and inductors are used for loading the underlying printed TLs. Experimental results of subdiffraction focusing and simulated wave propagation in the lens are also shown in Figure 6.

In an important new development, a fully isotropic Veselago-Pendry lens for microwaves has been constructed using stereolithography as reported in [23].

The main drawback of the Veselago-Pendry superlens is that the achieved superresolution is very sensitive to material losses [24]. A notable example for solving this problem is the so-called hyperlens, which utilizes anisotropic metamaterials that are characterized by a hyperbolic spatial dispersion diagram [25]–[26]. These hyperbolic media support tightly confined beams (akin to resonance cones in anisotropic plasmas), which have been demonstrated earlier at microwaves using TL metamaterials [27]. When these hyperbolic metamaterials are shaped into a cylindrical (or spherical) lens, then the beams that emanate from an object fan out, thus magnifying the subwavelength features; when they are separated by $\lambda/2$ or more, they can be observed using conventional far-field microscopy. Experimental demonstrations of this concept at optical frequencies using layered sliver/dielectric structures to synthesize the required hyperbolic metamaterials has been reported in [28] and [29]. Furthermore, it could be noted that, at microwave frequencies, hyperlenses have been built using a wire medium (parallel wires) as explained in [30]. Using this approach, it was demonstrated that the hyperlens acts as a translation device, moving an image and its subwavelength features from one plane to another. By making the wires diverging from each other with distance, this translation can be associated with a magnification at the image plane. The ability to obtain a magnified image along with a reduced sensitivity to material losses, highlights the potential benefits of using the hyperlens as an imaging device. However, the one drawback is that the working distance between the object and the lens must be very small compared to the free-space wavelength λ.

At microwave frequencies, hyperlenses have been built using a wire medium (parallel wires).

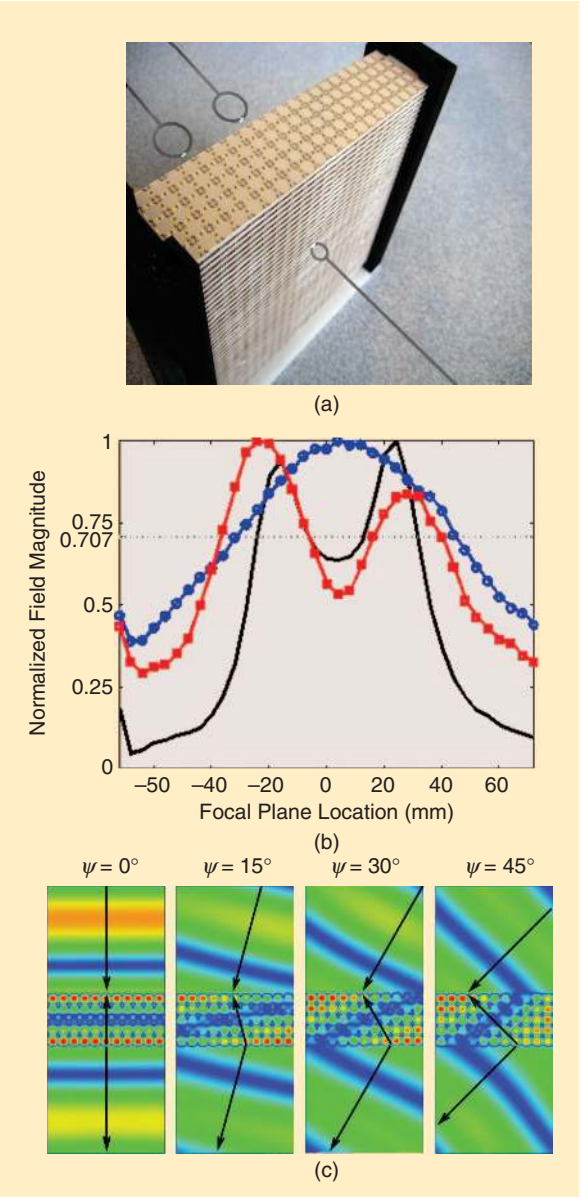

Figure 6. *(a) A free-space Veselago-Pendry NRI-TL superlens. Embedded chip capacitors and inductors are used to minimize losses. The slab consists of 5 cells × 21 cells × 43 layers ($w \times h \times t = 150\ mm \times 150\ mm \times 35.7\ mm$, period $d = 7\ mm$). (b) Super-resolving two sources that are spaced 40 mm apart at 2.4 GHz ($\lambda_o = 125\ mm$). The sources are magnetic dipoles (small current loops) having their axes perpendicular to the layers of the lens and placed at a distance $t/2 = 17.85\ mm$ from the lens.(c) Refraction of a plane-wave obliquely incident on the NRI-TL slab (full-wave simulations). Note the clear demonstration of negative refraction associated with the fundamental spatial harmonic β_{Bloch} (higher spatial harmonics $\beta_n = \beta_{\text{Bloch}} + 2\pi n/d$, $n = \pm 1, \pm 2, \pm 3, \ldots$ are all present in principle but they are weakly excited) [22].*

The beauty of TREM is that it enables a user-defined coordinate transformation to be translated into electric and magnetic material parameters.

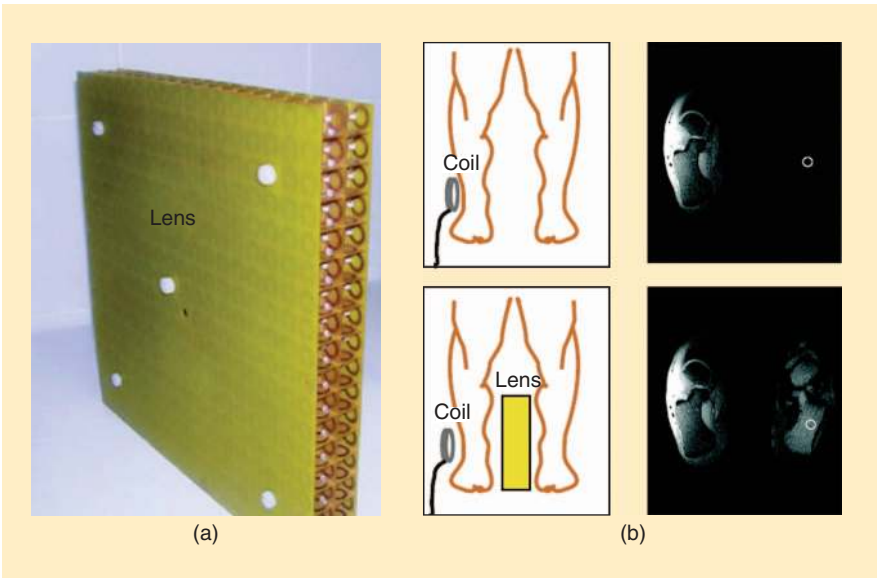

Figure 7. *(a) A negative permeability Veselago-Pendry lens made up of split-ring resonators used for MRI. (b) A diagram of the MRI experiment using the negative permeability lens. Without the lens, the RF fields far away from the lens cannot be seen by the surface coil. This result is demonstrated in an MRI of two ankles (cross section). With the lens the RF near fields are restored by the negative permeability lens allowing for both ankles to be imaged. (Images from [34], used with permission from Elsevier.)*

Another approach to alleviate the loss problems associated with the classical Veselago-Pendry lens has been developed in the past couple of years based on the so-called metascreens or meta-arrays and near-field plates, which can be thought of as superdirective arrays in the near field. For recent reviews, see [31] and [32]. In fact, the meta-array approach has the additional benefit that can alleviate the working distance constraint [31].

Application of a Superlens to MRI

An interesting application of metamaterials is to magnetic resonance imaging (MRI) where RF fields are crucial to the imaging process. During the image acquisition process, near-field signals are strongly prevalent as the various coils used in the imaging process all transmit and receive signals in the near field. MRI represents a potentially interesting application for metamaterials since metamaterial devices such as the Veslago-Pendry superlens are quite adept at manipulating near-field signals through restoring evanescent fields. One such interesting research thrust in applying metamaterials to MRI involves manipulating the near field of the surface with volumetric metamaterial lenses [33], [34]. In particular, this application involves the use of a negative permeability lens made out of split-ring resonators, which acts like a perfect lens in the quasistatic limit. From [20], it is noted that in the quasistatic limit, a slab of material with only a negative permittivity or a negative permeability will act like a perfect lens. Since the RF signals in MRI are sensed through a magnetic field and the field itself has a very long wavelength relative to the dimensions at hand, a quasistatic negative permeability lens may help in signal detection as it can restore the evanescent signals before they pass below the noise-floor. The setup used in [34] involves inserting a negative permeability lens made of split-ring resonators, shown in Figure 7(a), between a surface coil and the patient, as shown in Figure 7(b). This allows the surface coil and metamaterial to image further than what the surface coil by itself would accomplish. This is demonstrated in the MRI image shown in Figure 7(b), where the negative permeability lens placed between the ankles of the patient allows the surface coil to image both ankles, unlike the surface coil alone. Other research being carried out in this area includes using a wire-grid medium to channel MRI signals to ease detection of the signals from outside the MRI machine, as shown in [35].

Transformation Electromagnetics

At the beginning of this article, we posed the question "What would be possible if we were able to synthesize materials with user-defined constitutive parameters?" A definitive step toward answering this question has been provided by the development of transformation optics, which was first introduced in the seminal works [36] and [37]. In this article, we will instead use the term "transformation electromagnetics (TREM)," which is more general since it covers both microwaves and optics. In particular, TREM is based on the invariance of Maxwell's equations with respect to coordinate transformations. The beauty of TREM is that it enables a user-defined coordinate transformation to be translated into electric and magnetic material parameters, as will be outlined below following [38].

Geometry in Maxwell's Equations and its Relationship to Metamaterials

To understand the relationship between geometry and materials in Maxwell's equations, we consider two different spaces (See Figure 8):

- Maxwell's equations in free space referred to an arbitrary coordinate system. We will call this our transformed space.
- Maxwell's equations in an electric and magnetic medium referred to an arbitrary coordinate system. We will call this our material space.

In our first case, the transformed space, we are looking at an arbitrary coordinate system in free space. In such a context, the metric tensor is introduced, denoted by G, and it defines how distance in the corresponding arbitrary co-ordinate system is measured,

$$ds^2 = \sum_{i=1}^{3}\sum_{j=1}^{3} g_{ij}\, dx^i\, dx^j, \tag{6}$$

where dx^i are the differential lengths of the coordinate system and g_{ij} are the entries of G. This is a second-order tensor that has a determinant given by det(G). The inverse of the metric tensor is denoted by G^{-1}. The metric tensor characterizes all the geometrical properties of an arbitrary coordinate system [38]. When we write Maxwell's equations in a coordinate system with some metric tensor G, we find that the equations have an explicit dependence on the metric tensor. This is something that is hidden in the usual Cartesian frame of reference where the metric tensor is simply the identity matrix.

We now turn our attention to our second space, the material space, where we examine Maxwell's equations in a space filled with an electric and magnetic material $\overline{\overline{\varepsilon}}$ and $\overline{\overline{\mu}}$. Let us assume that this second space is defined by a coordinate system with a metric tensor given by Γ and a determinant given by det(Γ). We may recall that when we write Maxwell's equations in a space filled with an electric and magnetic material, we introduce the electric and magnetic flux densities. These flux densities are related to the fields through the constitutive relations. If we proceed to compare the two sets of Maxwell's equations in either space, as done in detail in [36], we can make an interesting observation: The two sets of equations can be made equivalent if the relative values of the electric and magnetic medium filling our second space have the following form:

If geometry and material parameters can be thought of as equivalent in Maxwell's equations, the next question to ask is what happens if we apply a coordinate transform to Maxwell's equations.

$$\overline{\overline{\varepsilon}} = \overline{\overline{\mu}} = \frac{\sqrt{\det(G)}}{\sqrt{\det(\Gamma)}}\, G^{-1}. \tag{7}$$

This allows us to state the following: Maxwell's equations in an arbitrary coordinate system in free space and Maxwell's equations in an electric and magnetic medium are equivalent if the material takes the form given in (7). Thus from the point of view of the fields, there is no difference between an arbitrary geometry as described by its metric tensor G and a material described by (7), as both sets of equations are describing the same fields.

Coordinate Transformations

If geometry and material parameters can be thought of as equivalent in Maxwell's equations, the next question to ask is what happens if we apply a coordinate transform to Maxwell's equations. We can look at how to interpret Maxwell's equations when transformed from one coordinate system to another, more specifically, interpreting the coordinate transform through the material parameters.

In the previous section, we introduced the transformed space. This space can be described via a

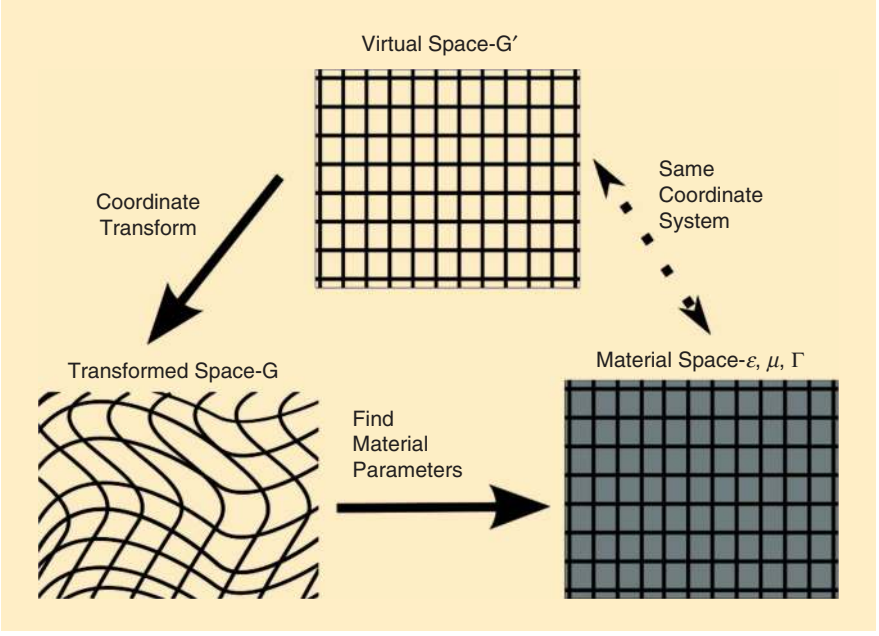

Figure 8. *The virtual space, the transformed space and the equivalent material space filled with an anisotropic material given by $\overline{\overline{\varepsilon}}$ and $\overline{\overline{\mu}}$.*

coordinate transformation from a simpler space (e.g., Cartesian, cylindrical, spherical). We refer to this simpler space as the virtual space. This virtual space is set in free space with a set of coordinates given by $\{x^{i'}, i' = 1, 2, 3\}$ and a metric tensor G'. We can then transform from the virtual space to the transformed space through a coordinate transform. Note that our transformed space is described by a set of coordinates $\{x^i, i = 1, 2, 3\}$ and, as stated previously, has a metric tensor G. To go from the virtual space to the transformed space, we formulate a coordinate transform given by $\{x^i = x^i(x^{i'}), i = 1, 2, 3\}$. This gives rise to the transformation matrix, Λ, whose entries are given by $\Lambda^i_{i'} = (\partial x^i)/(\partial x^{i'})$.

Now using this transformation matrix, we can write the inverse metric tensor of our transformed space in terms of the inverse metric tensor of the virtual space

$$G^{-1} = \Lambda G'^{-1} \Lambda^T. \tag{8}$$

Using the equivalence between geometry and material parameters that we established in the previous section, we can substitute (8) into (7), and with further simplification we get

$$\bar{\bar{\varepsilon}} = \bar{\bar{\mu}} = \frac{\sqrt{\det(G)}}{\sqrt{\det(\Gamma)}} \frac{\Lambda G'^{-1} \Lambda^T}{\det(\Lambda)}, \tag{9}$$

which is a set of material parameters that describe a corresponding coordinate transform. This well-known formula for TREM was first reported in [34] and establishes the connection between the coordinate transformation and the material parameters.

Note again what we have done. We started in our virtual space and used a coordinate transform to describe our transformed space. This allowed us to write the metric tensor of our transformed space in terms of our virtual space. We then wrote Maxwell's equations in our transformed space and interpreted the geometry of our transformed space as a set of material parameters. This takes us from our transformed space to our material space as given by (9), an expression which now depends on the transformation matrix of the coordinate transform. Recall also that our material space is situated in a coordinate system described by a metric tensor Γ. As it turns out, the coordinate system of our material space is of the same form as the coordinate system of our virtual space (Cartesian, cylindrical, spherical). See Figure 8 for a complete diagram.

Thus the set of material parameters in (9) allows us to implement the underlying coordinate transform without actually transforming the geometry! Instead, we simply use a material given by (9) and the fields will be transformed as they would have been if the geometry were actually transformed. This is what is referred to as the "material interpretation" [36]. Note that the material required to implement the coordinate transform is, in general, electrically and magnetically anisotropic (with off-diagonal tensor components) as well as inhomogeneous.

How to Make Something Disappear

We can formulate the aforementioned into a procedure, similar to [40], to give a framework for designing TREM devices. This framework uses three different spaces, as discussed previously, a virtual space, a transformed space, and a material space as follows:

1) We start with our virtual space, which we define with a coordinate system having a metric tensor G'. Usually it is a well-known coordinate system such as the Cartesian, cylindrical, or spherical systems.
2) We then formulate a coordinate transform to take us from our virtual space to our transformed space. We choose this coordinate transformation to implement the functionality of the device. For example, stretching or compressing space to control how electromagnetic waves will propagate through space or transforming a curved surface to a planar surface to alter the phase fronts of a wave.
3) We then use (9) to find a set of material parameters that we use to fill the material space, which is described by a coordinate system with a metric tensor Γ. This coordinate system is of the same form as in step 1 (Cartesian, cylindrical, spherical). Note that, as stated above, our material and transformed spaces are electromagnetically equivalent.

Example–The Cloak

The most popular transformation optics device is perhaps the cloak [36], [37]. The following uses the above procedure to design a cylindrical cloak:

1) Our virtual space is a cylindrical coordinate system given by $\{x^{i'} = r', \theta', z'\}$. The metric tensor of this space is given by $G' = \text{diag}\{1, r'^2, 1\}$ with a determinant $\det(G') = r'^2$. A picture of our virtual space is shown in Figure 9(a) .
2) We must now synthesize a cloak through a coordinate transform that describes the cloak's behavior. The purpose of the cloak is to guide electromagnetic waves around an object without scattering off the object itself. One way to do this is to compress the volume inside a cylinder of radius b into an annular region between a cylinder of radius b and a cylinder of radius a, where $a < b$. This is depicted in Figure 9(b). Any object placed inside the annular region between a and b in the transformed space is now protected from an impinging electromagnetic wave. This incoming electromagnetic wave, which would have traveled to the origin in the virtual space, travels instead around a cylinder of radius a. This is because the origin itself has been transformed to

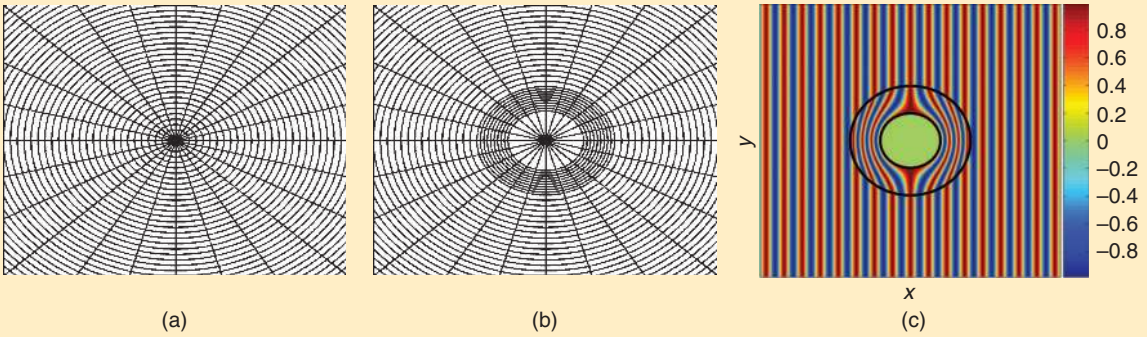

Figure 9. *(a) The virtual space for the cloak transformation, (b) the transformed space for the cloak (note how the space is compressed at the center), and (c) a plane wave traveling through the material space showing the functionality of the cloak.*

a cylinder of radius a. Mathematically, this transformation and its inverse are expressed as

$$x^i = \left\{ r(r') = r' \ \frac{b-a}{b} + a, \theta = \theta', \ z = z' \right\},$$
$$x^{i'} = \left\{ r'(r) = \frac{b(r-a)}{b-a}, \theta = \theta', z = z' \right\}, \qquad (10)$$

and the transformation matrix, $\Lambda^i_{i'} = (\partial x^i)/(\partial x^{i'})$, is given as $\Lambda = \text{diag}\{((b-a)/(b)), 1, 1\}$.

3) Finally, we find the required material parameters using (9). For the cylindrical cloak, we will express the material parameters in a cylindrical coordinate system, the same system used in step 1. The metric tensor of this system is given by $\Gamma = \text{diag}\{1, r^2, 1\}$. The parameters are then found to be

$$\overline{\overline{\varepsilon}} = \overline{\overline{\mu}} = \left\{ \frac{r-a}{r}, \frac{r}{r-a}, \left(\frac{b}{b-a}\right)^2 \frac{r-a}{r} \right\}. \qquad (11)$$

Note that the material parameters for the cloak are different from free space only in the annular region where the space has been transformed. Outside and inside the cloak, there is just free space. An example of the ideal fields inside the cloak can be seen in Figure 9(c) for the case of plane-wave incidence.

Building a Cloak

With the material parameters defined in (9), the next question that arises is implementation. How can one implement the material parameters given by a TREM device that require anisotropy and inhomogeneity? We can recognize that metamaterials are uniquely suited to this task as they can achieve the anisotropy and inhomogeneity required by the TREM material parameters. For the example of the cloak, this was first accomplished using split-ring resonators to construct a 2-D cylindrical cloak [39]. Approximations were made in the design to minimize the anisotropy of the device, whereas the inhomogeneity of the device was implemented by varying the dimensions of the split-ring resonators across the radius of the device, as shown in Figure 10. A plot of the measured field is also shown in Figure 10.

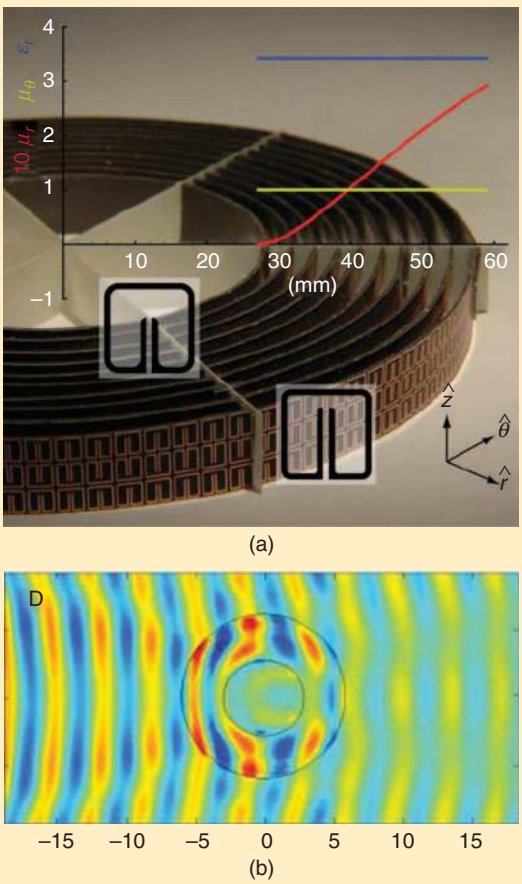

Figure 10. *(a) A fabricated cloak using split-ring resonators. (b) A plot of the measured fields of the cloak built using split-ring resonators. (Both images from [39], with permission from the AAAS.)*

The introduction of TREM has spurred a lot of work into developing further extensions of the main concept as well as further experimental work.

TL metamaterials have also been proposed to design TREM devices such as cloaks. Because of the grid-like nature of TL metamaterials, novel unit cells with additional loading are needed to implement the anisotropy of the material parameters in Cartesian coordinates [40], [41]. Examples of these unit cells and the cloaks designed using them are shown in Figure 11. As was pointed out earlier, TL metamaterials in general lead to broader bandwidths and smaller transmission losses [19].

The TREM paradigm for TL networks such as those shown in Figure 11 highlights a few salient features. 1) Metamaterials need not be periodic structures, they can be inhomogeneous, and 2) the control of the fields (voltages and currents) is achieved in the spatial domain. This brings out an important difference between TL metamaterials and traditional electrical networks and filters. Unlike electrical networks and filters, which primarily control voltage and current quantities in the frequency domain, metamaterials control the electromagnetic field distribution in the spatial domain.

Further Work In Transformation Electromagnetics

The introduction of TREM has spurred a lot of work into developing further extensions of the main concept

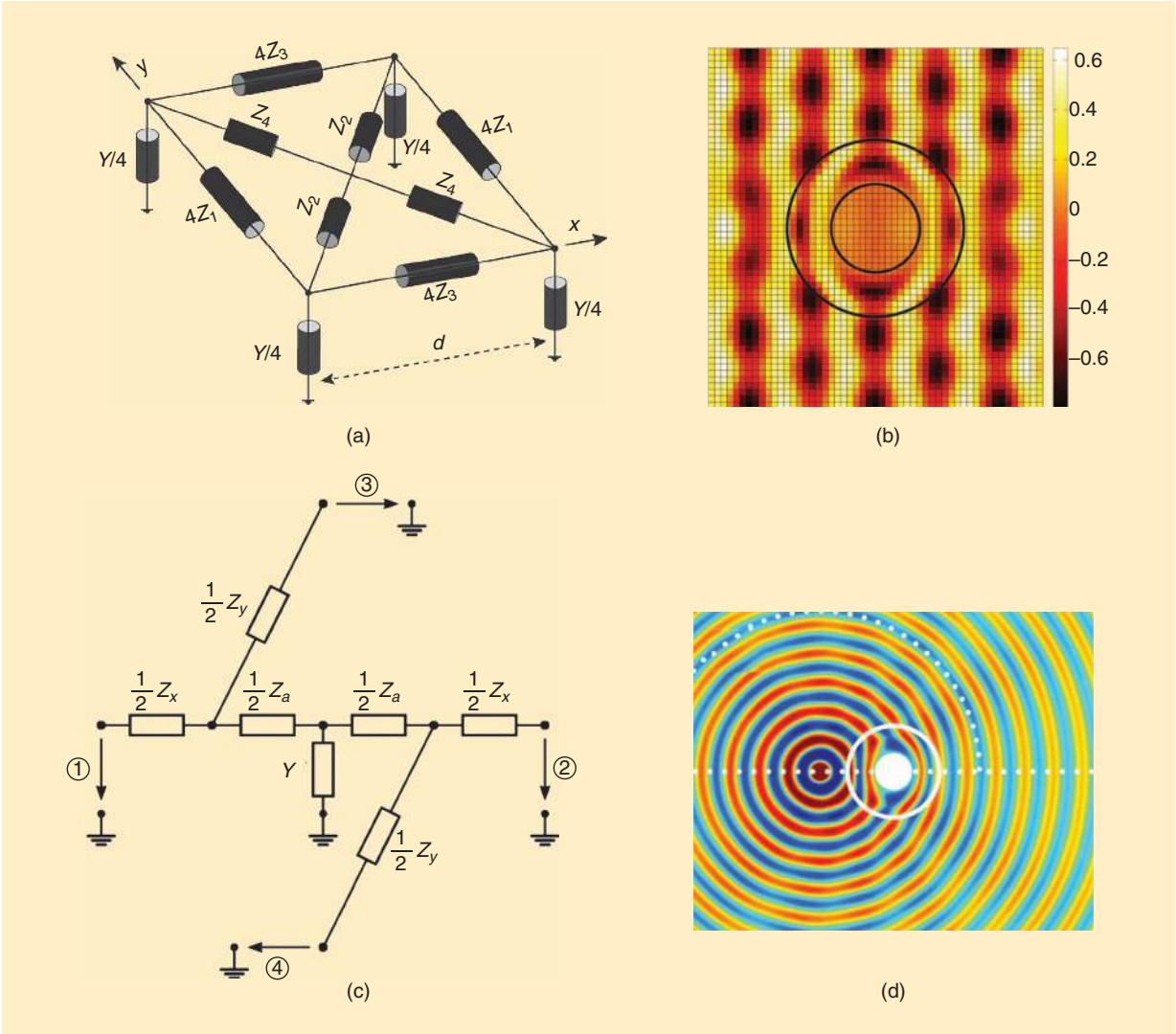

Figure 11. *(a) A TL metamaterial unit cell for implementing full material tensors. Taken from [40]. (b) A plot of the simulated fields in the cloak using the unit cell in (a). Taken from [40]. (c) A TL metamaterial unit cell for implementing full material tensors. Taken from [41]. (d) A plot of the simulated fields in the cloak using the unit cell in (c). Taken from [41]. Using the TL metamaterial approach allows one to achieve better performance than the SRR approach. As shown in [41], the TL cloak achieves a total radar cross section reduction of 12.8 dB and a bandwidth of 33%.*

as well as further experimental work. For example, the TREM concept discussed above has given rise to a variety of novel designs for electromagnetic devices. Using various coordinate transforms, designs have been proposed for devices such as beam expanders and beam splitters [42]–[44]. Other devices, such as a radome, which improves the scan range of a phased array [45], and an omnidirectional retroreflector (Eaton's lens) [46], have been designed and also fabricated and tested.

The theory of TREM has been extended to use different coordinate transformation techniques. One key development that improves on the concept is that of quasiconformal transformations, discussed in [47]–[49]. This approach minimizes the anisotropy of the material parameters by using transformations that keep the transformed grid lines as close to orthogonal as possible. A variety of devices have been proposed that use this quasiconformal transformation technique. These include a ground-plane cloak, which hides an object placed over a metallic ground plane [47], [50], a flat Luneburg Lens [51], and a flat dielectric lens [52]. Due to the material simplicity allowed by the quasiconformal technique, all of these examples have been fabricated and tested.

While this is only a sampling of some current work, TREM with metamaterials presents a large opportunity to envision, design and create novel kinds of electromagnetic devices.

Conclusion

The emerging field of metamaterials can be thought of as a rebirth of the field of artificial dielectrics that formally originated in the 1940s and 1950s in the microwave regime. However, with metamaterials, one seeks to synthesize unusual electromagnetic properties such as a negative permittivity, a negative permeability, or nearly zero or very large values of those, and so on. Especially in the optical regime, such concepts had never been applied before, and they enabled the synthesis of artificial media with difficult-to-obtain properties such as a magnetic response. These developments are now becoming meaningful because of substantial improvements in nanofabrication. On the other hand, at microwave frequencies, metamaterials opened a new avenue for innovation, leading to novel devices and antennas [18], [53]–[55]. For a recent collection of papers on the latest developments in metamaterials at both the microwave and optical domains, see the October 2011 issue of *Proceedings of the IEEE* [56].

More recently, the very powerful technique of TREM has been developed for designing with metamaterials. As was explained in this article, TREM can be utilized for the total control of the electromagnetic fields in materials. Given a valid coordinate transformation, TREM predicts the required material tensors

The emerging field of metamaterials can be thought of as a rebirth of the field of artificial dielectrics that formally originated in the 1940s and 1950s.

$\overline{\overline{\varepsilon}}(x, y, z)$ and $\overline{\overline{\mu}}(x, y, z)$ to control wave propagation at will. A derived application that captured much attention early on was cloaking, but currently, many more novel and useful applications are emerging, some of which have been mentioned in this article.

We finish this article by charting out an interesting problem for the microwave field/network engineer: TREM prescribes a method for the spatial control of the electromagnetic fields (or for the voltages and currents in TL metamaterials). However, the fundamental issue of the frequency bandwidth of the resulting TREM metamaterials is not explicitly treated. Obviously, bandwidth issues are crucial for many applications, including cloaks, flat and specialty lenses, etc. To this end, the marriage of TREM with classical network/filter theory may show the way to significantly improve TREM theory to enable the development of even more practical devices and structures in the future.

References

[1] L. Brillouin, *Wave Propagation in Periodic Structures*. New York: Dover, 2003.

[2] W. Kock, "Metallic delay lenses," *Bell Syst. Tech. J.*, vol. 27, pp. 58–82, 1948.

[3] R. E. Collin, *Field Theory of Guided Waves. Piscataway*, NJ: IEEE Press, 1990, ch. 12.

[4] J. C. Bose, "On the rotation of plane of polarization of electric waves by a twisted structure," *Proc. R. Soc.*, vol. 63, pp. 146–152, 1898.

[5] I. V. Lindell, A. H. Sihvola, and J. Kurkijarvi, "Karl F. Lindman: The last Hertzian, and a harbinger of electromagnetic chirality," *IEEE Antennas Propagat. Mag.*, vol. 34, no. 3, pp. 24–30, 1992.

[6] A. von Hippel, *Dielectrics and Waves*. Artech House, Boston, 1995.

[7] V. G. Veselago, "The electrodynamics of substances with simultaneously negative values of ϵ and μ," *Soviet Physics Usphekhi*, vol. 10, no. 4, pp. 509–514, 1968.

[8] R. A. Shelby, D. R. Smith, S. Schultz, "Experimental verification of a negative index of refraction," *Science*, vol. 292, pp. 77–79, Apr. 2001.

[9] W. Rotman, "Plasma simulation by artificial dielectrics and parallel-plate media," *IRE Trans. Antennas Propagat.*, vol. 10, pp. 82–95 Jan. 1962.

[10] J. B. Pendry, A. J. Holden, W. J. Stewart, and I. Youngs, "Extremely low frequency plasmons in metallic mesostructures," *Phys. Rev. Lett.*, vol. 76, no. 25, pp. 4773–4776, 1996.

[11] J. B. Pendry, A. J. Holden, D. J. Robbins, and W. J. Stewart, "Magnetism from conductors and enhanced nonlinear phenomena," *IEEE Trans. Microwave Theory Tech.*, vol. 47, pp. 2075–2084, Nov. 1999.

[12] S. A. Schelkunoff and H.T. Friis, *Antennas: Theory and Practice*. New York: Wiley, 1952.

[13] G. V. Eleftheriades, A. K. Iyer, and P. C. Kremer, "Planar negative refractive index media using periodically L-C loaded transmission

lines," *IEEE Trans. Microwave Theory Tech.*, vol. 50, no. 12, pp. 2702–2712, Dec. 2002.

[14] A. Sanada, C. Caloz, and T. Itoh, "Planar distributed structures with negative refractive index," *IEEE Trans. Microwave Theory Tech.*, vol. 52, no. 4, pp. 1252–1263, Apr. 2004.

[15] A. Oliner, "A planar negative-refractive-index medium without resonant elements," in *IEEE MTT-S Int. Microwave Symp. Dig.*, Philadelphia, PA, July 2003, vol. 1, pp. 191–194.

[16] M. Zedler and G. V. Eleftheriades, "Spatial harmonics and homogenization of negative-refractive-index transmission-line structures," *IEEE Trans. Microwave Theory Tech.*, vol. 58, no. 6, pp. 1521–1531, June 2010.

[17] A. Grbic and G. V. Eleftheriades, "Periodic analysis of a 2-d negative refractive index transmission line structure," *IEEE Trans. Antennas Propagat.*, vol. 51, no. 10, pp. 2604–2611, Oct. 2003.

[18] G. V. Eleftheriades and K. G. Balmain, Eds., *Negative-Refraction Metamaterials*. New York: Wiley-IEEE Press, 2005.

[19] G. V. Eleftheriades, "Analysis of bandwidth and loss in negative-refractive-index transmission-line (NRI-TL) media using coupled resonators," *IEEE Microwave Wireless Compon. Lett.*, vol. 17, pp. 412–414, June 2007.

[20] J. B. Pendry, "Negative refraction makes a perfect lens," *Phys. Rev. Lett.*, vol. 85, no. 18, pp. 3966–3969, Oct. 2000.

[21] A. Grbic and G. V. Eleftheriades, "Overcoming the diffraction limit with a planar left-handed transmission-line lens," *Phys. Rev. Lett.*, vol. 92, no. 11, pp. 117403–117406, Mar. 2004.

[22] K. Iyer and G. V. Eleftheriades, "Free-space imaging beyond the diffraction limit using a Veselago-Pendry transmission-line metamaterial superlens," *IEEE Trans. Antennas Propagat.*, vol. 57, pp. 1720–1727, June 2009.

[23] S. M. Rudolph and A. Grbic, "A broadband three-dimensional isotropic negative-refractive-index medium," in *Proc. IEEE Antennas Propagat. Int. Symp.*, July 2010, pp. 1–4.

[24] D. R. Smith, D. Schurig, M. Rosenbluth, S. Schultz, S. A. Ramakrishna, and J. B. Pendry, "Limitations on subdiffraction imaging with a negative refractive index slab," *Appl. Phys. Lett*, vol. 82, no. 10, pp. 1506–1508, 2003.

[25] A. Salandrino and N. Engheta, "Far-field subdiffraction optical microscopy using metamaterial crystals: Theory and simulations," *Phys. Rev. B*, vol. 74, no. 7, p. 075103–075107, Aug. 2006.

[26] Z. Jacob, L. V. Alekseyev, and E. Narimanov, "Optical hyperlens: Far-field imaging beyond the diffraction limit," *Opt. Express*, vol. 14, no. 18, pp. 8247–8256, 2006.

[27] K. G. Balmain, A. A. E. Lüttgen, and P. C. Kremer, "Resonance cone formation, reflection, refraction, and focusing in a planar anisotropic metamaterial," *IEEE Antennas Wireless Propagat. Lett.*, vol. 1, no. 7, pp. 146–149, 2002.

[28] I. I. Smolyaninov, Y. J. Hung, and C. C. Davis, "Magnifying superlens in the visible frequency range," *Science*, vol. 315. no. 5819, pp. 1699–1701, Mar. 2007.

[29] Z. Liu, H. Lee, Y. Xiong, C. Sun, and X. Zhang, "Far-field optical hyperlens magnifying sub-diffraction-limited objects," *Science*, vol. 315, no. 1686, 2007.

[30] Y. Zhao, G. Palikaras, P. A. Belov, R. F. Dubrovka, C. R. Simovksi, Y. Hao, and C. G. Parini, "Magnification of subwavelength field distributions using a tapered array of metallic wires with planar interfaces and an embedded dielectric phase compensator," *New J. Phys.*, vol. 12, no. 10, p. 103045–103055, 2010.

[31] L. Markley and G. V. Eleftheriades, "Meta-screens and near-field antenna-arrays: A new perspective on subwavelength focusing and imaging," *Metamaterials*, vol. 5, nos. 2–3, pp. 97–106, June–Sept. 2011.

[32] A. Grbic and R. Merlin, "Near-field plates: Metamaterial surfaces/arrays for subwavelength focusing and probing," *Proc. IEEE*, vol. 99, no. 10, pp. 1806–1815, Oct. 2011.

[33] M. J. Freire, R. Marques, and L. Jelinek, "Experimental demonstration of a $\mu = -1$ metamaterial lens for magnetic resonance imaging," *Appl. Phys. Lett.*, vol. 93, no. 23, p. 231108–231110, 2008.

[34] M. J. Freire, L. Jelinek, R. Marques, and M. Lapine, "On the applications of $\mu_r = -1$ metamaterial lenses for magnetic resonance imaging," *J. Magn. Reson.*, vol. 203, no. 1, pp. 81–90, 2010.

[35] C. Xavier Radu and D. Garray, "Toward a wire medium endoscope for MRI imaging," *Metamaterials*, vol. 3, no. 2, pp. 90–99, 2009.

[36] J. B. Pendry, D. Schurig, and D. R. Smith, "Controlling electromagnetic fields," *Science*, vol. 312, pp. 1780–1782, June 2006.

[37] U. Leonhardt, "Optical conformal mapping," *Science*, vol. 312. no. 5781, pp. 1777–1780, June 2006.

[38] U. Leonhardt and T. Philbin, *Geometry and Light: The Science of Invisibility*. New York: Dover, 2010.

[39] Schurig, J. J. Mock, B. J. Justice, S. A. Cummer, J. B. Pendry, A. F. Starr, and D. R. Smith, "Metamaterial electromagnetic cloak at microwave frequencies," *Science*, vol. 314, no. 5801, pp. 977–980, 2006.

[40] G. Gok and A. Grbic, "Tensor transmission-line metamaterials," *IEEE Trans. Antennas Propagat.*, vol. 58, no. 5, pp. 1559–1566, May 2010.

[41] M. Zedler and G. V. Eleftheriades, "Anisotropic transmission-line metamaterials for 2-D transformation optics applications," *Proc. IEEE*, vol. 99, no. 10, pp. 1634–1645, Oct. 2011.

[42] Kwon and D. Werner, "Transformation electromagnetics: An overview of the theory and applications," *IEEE Antennas Propagat. Mag.*, vol. 52, no. 1, pp. 24–46, 2010.

[43] M. Rahm, D. A. Roberts, J. B. Pendry, and D. R. Smith, "Transformation-optical design of adaptive beam bends and beam expanders," *Opt. Express*, vol. 16, no. 15, pp. 11555–11567, July 2008.

[44] D. Emiroglu and D.-H. Kwon, "Impedance-matched three-dimensional beam expander and compressor designs via transformation optics," *J. Appl. Phys.*, vol. 107, no. 8, p. 084502–084507, 2010.

[45] T. A. Lam, D. C. Vier, J. A. Nielsen, C. G. Parazzoli, and M. H. Tanielian, "Steering phased array antenna beams to the horizon using a buckyball NIM lens," *Proc. IEEE*, vol. 99, no. 10, pp. 1755–1767, Oct. 2011.

[46] Y. G. Ma, C. Ong, T. Tyc, and U. Leonhardt, "An omnidirectional retroreflector based on the transmutation of dielectric singularities," *Nature Mater.*, vol. 8, no. 8, pp. 639–642, 2009.

[47] J. Li and J. B. Pendry, "Hiding under the carpet: A new strategy for cloaking," *Phys. Rev. Lett.*, vol. 101, no. 20, p. 203901–203903, Nov. 2008.

[48] W. Tang, C. Argyropoulos, E. Kallos, W. Song, and Y. Hao, "Discrete coordinate transformation for designing all-dielectric at antennas," *IEEE Trans. Antennas Propagat.*, vol. 58, no. 12, pp. 3795–3804, 2010.

[49] N. B. Kuntz, D. R. Smith, Y. Urzhumov and N. I. Landy, "Enhancing imaging systems using transformation optics," *Opt. Express*, vol. 18, no. 20, pp. 21238–21251, 2010.

[50] R. Liu, C. Ji, J. J. Mock, J. Y. Chin, T. J. Cui, and D. R. Smith, "Broadband ground-plane cloak," *Science*, vol. 323, no. 5912, pp. 366–369, 2009.

[51] N. Kundtz and D. R. Smith, "Extreme-angle broadband metamaterial lens," *Nature Mater.*, vol. 9, no. 2, pp. 129–132, 2010.

[52] R. Yang, W. Tang, Y. Hao, and I. Youngs, "A coordinate transformation-based broadband flat lens via microstrip array," *IEEE Antennas Wireless Propagat.* Lett., vol. 10, pp. 99–102, 2011.

[53] N. Engheta and R.W. Ziolkowski, Eds., *Electromagnetic Metamaterials: Physics and Engineering Explorations*. New York: Wiley-IEEE Press, July 2006.

[54] Caloz and T. Itoh, Electromagnetic Metamaterials: Transmission Line Theory and Microwave Applications. New York: Wiley-IEEE Press, 2006.

[55] R. Marqués, F. Martín, and M. Sorolla, Metamaterials with Negative Parameters: Theory, Design and Microwave Applications. New York: Wiley, Jan. 2008.

[56] G. V. Eleftheriades and N. Engheta, "Metamaterials: Fundamentals and applications in the microwave and optical regimes, scanning the issue (editorial)," *Proc. IEEE*, vol. 99, no. 10, pp. 1618–1621, Oct. 2011.

[57] G. V. Eleftheriades, "EM Transmission-line metamaterials," *Materials Today*, vol. 12, p. 3041, Mar. 2009.